THE USE OF DIGITAL IMAGE CORRELATION TECHNIQUE FOR MONITORING MASONRY ARCH BRIDGES

Iris S. Koltsida*, Adrienn K. Tomor*, Colin A. Booth*

* University of the West of England, Faculty of Technology and Environment, Bristol, UK
Iris.Koltsida@uwe.ac.uk, Adrienn.Tomor@uwe.ac.uk & Colin.Booth@uwe.ac.uk

Keywords: Digital Image Correlation, NDT, monitoring, masonry arch bridges, crack propagation

ABSTRACT

Non-destructive monitoring of the infrastructure is becoming an increasingly important issue for asset management. Masonry arch bridges represent around 40% of the European bridge stock, many of them over 100 years old and in increasing need for maintenance. Condition assessment of masonry arch bridges relies largely on visual observation, although a range of non-destructive techniques (NDT) are available for monitoring their condition and performance. Identifying deterioration and changes in the structure's behaviour under working loads would be of great help to prevent critical damage. While most NDT techniques require direct access to the structure and can be labour-intensive, Digital Image Correlation (DIC) technique offers a low-cost optical solution that allows surface displacement, stress and strain distribution to be recorded without any contact with the structure. Digital Image Correlation is increasingly widely used for civil infrastructure, but its use for masonry arch bridges is currently rather limited. The paper demonstrates the use of Digital Image Correlation technique under laboratory conditions for small-scale masonry specimens and under field conditions for a masonry arch railway bridge under traffic loading.

1. INTRODUCTION

Non-destructive monitoring of the infrastructure is becoming an increasingly important issue for asset management. Masonry arch bridges represent around 40% of the European bridge stock, many of them over 100 years old and in increasing need for maintenance. Condition assessment of masonry arch bridges relies largely on visual observation, although a range of non-destructive techniques (NDT) are available for monitoring their condition and performance [1-4]. Identifying deterioration and changes in the structure's behaviour under working loads would be of great help to prevent critical damage. While most NDT techniques require direct access to the structure and can be labour-intensive, Digital Image Correlation (DIC) technique offers a low-cost optical solution that allows surface displacement, stress and strain distribution to be recorded without any contact with the structure [5-6]. Digital Image Correlation is increasingly widely used for civil infrastructure, but its use for masonry arch bridges is currently rather limited. The paper demonstrates the use of Digital Image Correlation technique under laboratory conditions for small-scale masonry specimens and under field conditions for a masonry arch railway bridge under traffic loading.

2. DIGITAL IMAGE CORRELATION THEORY

Digital Image Correlation (DIC) is an optical measurement technique that has been widely used to study surface deflection, strain and stress distribution in various building materials. The method combines continuous recording of horizontal and vertical displacement with no direct contact with the sample, excluding any interference between the measured surface and the measuring device [7]. DIC is based on tracking two dimensional in-plane local deformation between two surface images. A reference picture is captured before loading and a series of pictures are taken subsequently during the loading process. The area of interest is defined on the reference image that is subsequently divided into smaller image subsets. The greyscale intensity within the subsets needs to be unique to be tracked from one image to the next [7].

To identify similar patterns between the reference and target subsets, a cross-correlation (CC) or sum-squared difference (SSD) correlation criterion is adapted (Bing et al., 2009). The matching procedure is completed through searching the peak position where the distribution of the correlation coefficient is the highest. When the maximum correlation coefficient is located, the position of the deformed subset is determined (Figure 1). The differences in the positions of the reference subset centre and the target subset centre provide the in-plane displacement vector [8].

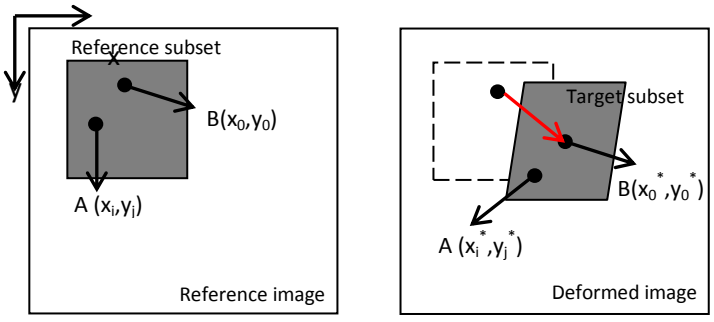

Figure 1: Reference square subset before deformation and a target subset after deformation

The cross-correlation coefficient (r_{CC}) is given by Equation 1:

$$r_{cc} = 1 - \frac{\Sigma_i \Sigma_j \left[F(x_i y_j) - \bar{F}\right]\left[G(x_i^*, y_j^*) - \bar{G}\right]}{\sqrt{\Sigma_i \Sigma_j \left[F(x_i y_j) - \bar{F}\right]^2 \Sigma_i \Sigma_j \left[G(x_i^*, y_j^*) - \bar{G}\right]^2}} \quad (1)$$

where $F(x_i, y_j)$ is the pixel intensity or the gray scale value at a point (x_i, y_j) in the undeformed image and $G(x_i^*, y_j^*)$ is the gray scale value at a point (x_i^*, y_j^*) in the deformed image. $\bar{F}$ and $\bar{G}$ are the mean values of the intensity matrices F and G, respectively. The coordinates or grid points (x_i, y_j) and (x_i^*, y_j^*) are related by the deformation that occurs between acquisition of the two images. If the deformation during the experiment is parallel to the xy-plane of the image, co-ordinates are related by (Equations 1-2):

$$x^* = x + u + \frac{\vartheta u}{\vartheta x}\Delta x + \frac{\vartheta u}{\vartheta y}\Delta y \quad (2)$$

$$y^* = y + v + \frac{\vartheta v}{\vartheta x}\Delta x + \frac{\vartheta v}{\vartheta y}\Delta y \quad (3)$$

where u and v are translations of the center of the sub-image in the X and Y directions, respectively. The distances from the center of the sub-image to the point (x, y) are denoted by Δx and Δy. Thus, the correlation coefficient r_{CC} is a function of displacement components (u, v) and displacement gradients.
The strain field calculation is performed using the Green-Lagrange strain tensor given by Equation 4:

$$E = \frac{1}{2}(F^T F - I) \quad (4)$$

where F is the deformation gradient tensor and I is a unit matrix [7].

The Green-Lagrange strain tensor can be written explicitly in terms of components of displacement (Equations 6-8):

$$\varepsilon_{xx} = \frac{\vartheta u}{\vartheta x} + \frac{1}{2}\left[\left(\frac{\vartheta u}{\vartheta x}\right)^2 + \left(\frac{\vartheta v}{\vartheta x}\right)\right] \quad (6)$$

$$\varepsilon_{yy} = \frac{\vartheta v}{\vartheta y} + \frac{1}{2}\left[\left(\frac{\vartheta v}{\vartheta y}\right)^2 + \left(\frac{\vartheta u}{\vartheta y}\right)^2\right] \quad (7)$$

$$\varepsilon_{xy} = \frac{1}{2}\left[\frac{\vartheta u}{\vartheta y} + \frac{\vartheta v}{\vartheta x} + \frac{\vartheta u \vartheta u}{\vartheta x \vartheta y} + \frac{\vartheta v \vartheta v}{\vartheta x \vartheta y}\right] \quad (8)$$

The technique exhibits several important advantages that make it suitable for both laboratory and field applications. Experimental setup and specimen preparation are quick, easy and low-cost (Figure 2a), requiring only a fixed CCD camera, a white light source (or natural light) and sprayed speckle pattern applied to the specimen's surface (in certain cases). An artificial speckle is not required for masonry, as the natural texture of the specimen's surface has random grey intensity distribution. The technique provides a wide-range of measurement sensitivity and resolution options and can be coupled to a range of different techniques [8]. The accuracy of the method can however be influenced by changes in the lighting conditions during subsequent images, difficulties in detecting the correct position of the subset, camera movements, vibration, etc. The correlation function may also lead to errors in the region of rough edges, i.e. intersection of the specimen with the background [9].

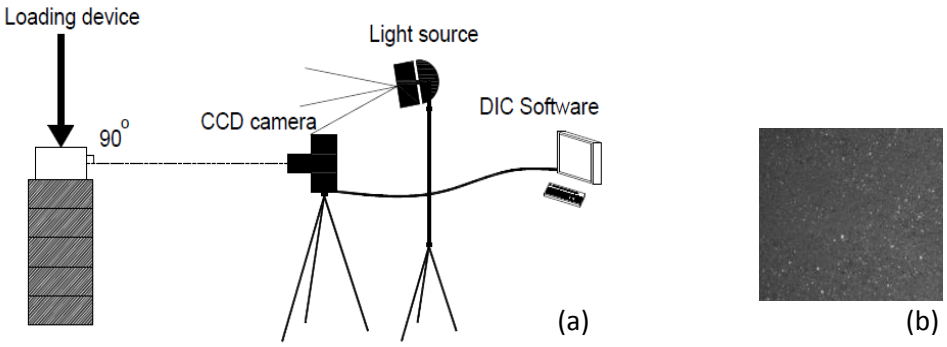

Figure 2: (a) Digital Image Correlation experimental setup and (b) natural texture of clay bricks

3. USING DIGITAL IMAGE CORRELATION TO MONITOR LABORATORY TESTS ON BRICKS

3.1. Test setup

In order to evaluate the potentials and limitations of the Digital Image Correlation technique for monitoring masonry under laboratory conditions, a series of clay brick units have been tested at the University of the West of England, UK under static loading. Soft solid clay bricks (210x100x65mm^3) were selected with 1400 kg/m^3 density and 6 N/mm^2 compressive strength that may be representative of the bricks found in waterways bridges. The bricks were tested under compression with displacement control using a 250 kN actuator between 3 mm plywood and 30 mm thick steel plates. The displacement rate was 10 nm/sec up to 70 kN and subsequently decreased to 2 nm/sec to record post peak behaviour.

3.2. Instrumentation

2D Digital Image Correlation was used to obtain the surface displacement and strain field during different phases of the loading. A Nikon D3100 DSLR of 14 megapixel resolution camera with Nikon AF-S DX Micro NIKKOR 40 mm f/2.8G lens with a field view (to cover the entire specimen) was placed perpendicular to the monitored surface of the specimen. A shutter remote control was used to take the images to avoid camera movement and lighting was provided by a continuous Photo Video Studio focusable Redhead spot light.
No artificial speckle was applied on the brick's surface as mentioned before, as the natural texture of the specimen's surface already had a random grey intensity distribution due to the inhomogeneity of the material (Figure 2b).
A reference image was taken before the experiment and pictures were recorded at every 1kN load increment. The analysis of the results as well as the calibration of the camera was performed using MatchID-2D software [10], developed by the Mechanical Engineering department of the Catholic University College Ghent. The software is able to record deflection or strain across the surface area or for any of its subsections.
Two Linear Variable Differential Transformers (LVDTs) were placed at the right and left hand side of the bricks to monitor deformations across the height of the brick while images were taken of the front of the bricks only.

3.3. Results

3.3.1. Measuring displacement

Displacement measured by DIC as the average of the overall surface area (A) and a smaller uncracked area near the left hand side (B) are compared with the average of the two LVDTs (C) against load in Figure 4. For the elastic range (< 10% load) the DIC and LVDT measurements are identical. During the plastic range (10% - 87% load) the LVDTs show somewhat higher displacement, however the small uncracked area B shows a closer resemblance to the LVDTs. This is not unexpected, as the DIC readings over area A include the entire brick surface and any change in behaviour would be averaged over a larger surface, becoming less significant. A sudden change around 87% load (associated with part of the brick breaking off) is clearly visible by the LVDTs but less so by the DIC measurements for the same reasons. Differences are also attributed to the fact that the LVDTs are measuring the average displacement on the left and left edges of the brick, while DIC areas A and B the front of the brick.

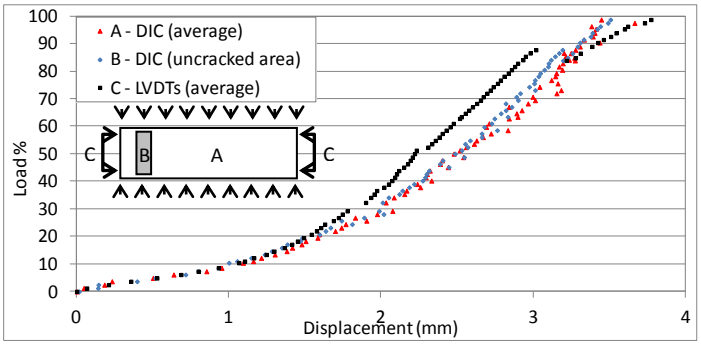

Figure 3: Load vs. displacement measured by DIC, LVDTs (average of two sensors) and DIC

3.3.2. Measuring strain and locating cracks

In terms of measuring strain, displacement and crack location, examples of the displacement and strain fields at 50% and 100% of the ultimate load are shown in Figures 5a-d. In the x and y displacement fields cracks can be identified where the contour colours change sharply. For example, a single major vertical crack is seen across the whole height of the specimen around the middle of the brick by a sharp change in colour. A cluster of smaller cracks is however indicated by a range of colours in the lower right corner of the brick. Principal strain fields (Figures 5c-d) display similar characteristics to deflections, however make distinguishing individual or clusters of cracks more difficult.

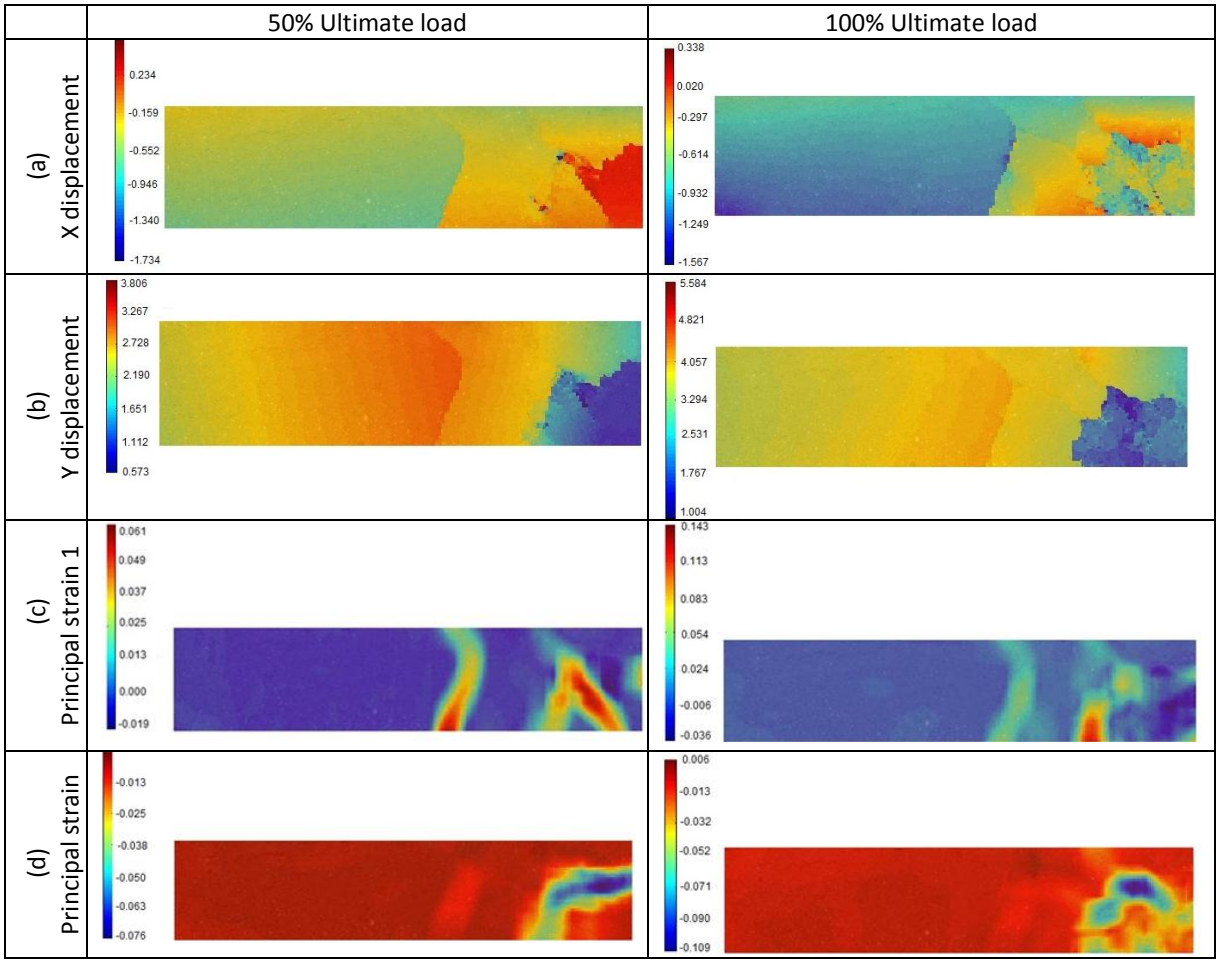

Figure 4**:** x, y displacements and principal strains

3.3.3. Measuring crack opening

Once presence of cracks is identified, DIC can be easily used to measure crack opening. In Figure 5 the opening of the large vertical crack near the middle of the brick is shown at two locations (across two pairs of points A-A and B-B) against load. For both locations a sharp increase in the relative displacement is visible up to 10% of the ultimate load, after which the displacement remains relatively stable and the crack fully open. The displacement reduces again from around 80% load, indicating change in the behaviour of the material. A sudden change in the load-displacement measurement was also identified by the LVDTs around 87% load in Figure 3 that is likely to be associated with the same phenomenon. Although the DIC surface measurement was less informative in Figure 3, the DIC crack measurement appears to provide a much more accurate tool for indicating change in behaviour at an earlier stage.

The greater displacement at location A compared to B throughout the entire test indicates that crack propagation initiated from the bottom edge of the brick and led to development of a hinge. Subsequent visual observation

confirmed that the brick was slightly bowed initially and only the bottom left and right edges were touching the base plate, causing bending of the brick and a vertical crack/hinge development at the start of load application (<10% load).

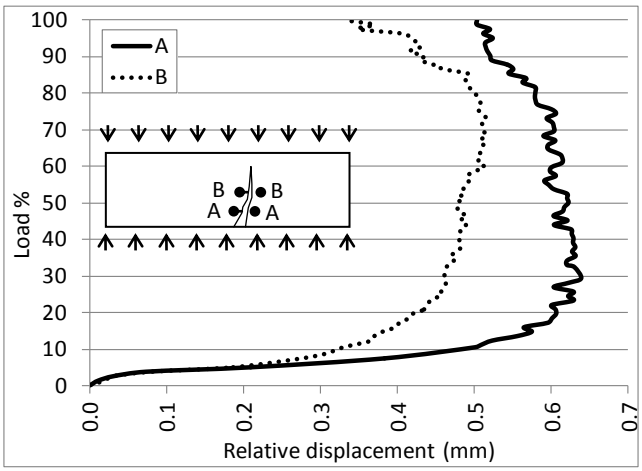

Figure 5: Load vs. relative displacement during crack propagation

4. FIELD MONITORING

In order to study the efficacy of Digital Image Correlation for field monitoring, a pilot test has been carried out on a four-span railway bridge (Figure 6) under normal traffic loading. The bridge shows some signs of deterioration and evidence for a range of historical strengthening measures.

Figure 6: Railway bridge with the monitored area

The instrumentation for Digital Image Correlation used for monitoring the bridge was the one also used for the laboratory experiments. Examples of DIC output for a British Rail Class 220 train (weight ca. 45 tonnes per bogie, maximum speed 200 km/h) is shown in Figure 7 for the 1st and the 2nd spans of the bridge monitored from ca. 10 m distance. Figure 7a-e shows the horizontal and vertical displacements fields as the train was driving over the bridge. In Figure 9a the train just entered the 1st and 2nd spans (from the left) and some movement is indicated towards the right and downwards in both spans. While the train is over both spans (Figures 9b, c) similar movements (towards the right and downwards) are indicated. As the train just left the 1st span but it is still over the 2nd and subsequent spans (Figure 9d), the 2nd span is starting to move towards the left and both spans starting to move upwards. It is slightly surprising that the 1st span is still moving towards the right. Finally, as the train has just left both spans (Figure 9e), the 2nd span moves again towards the right and both continue moving upwards, recovering their original positions.

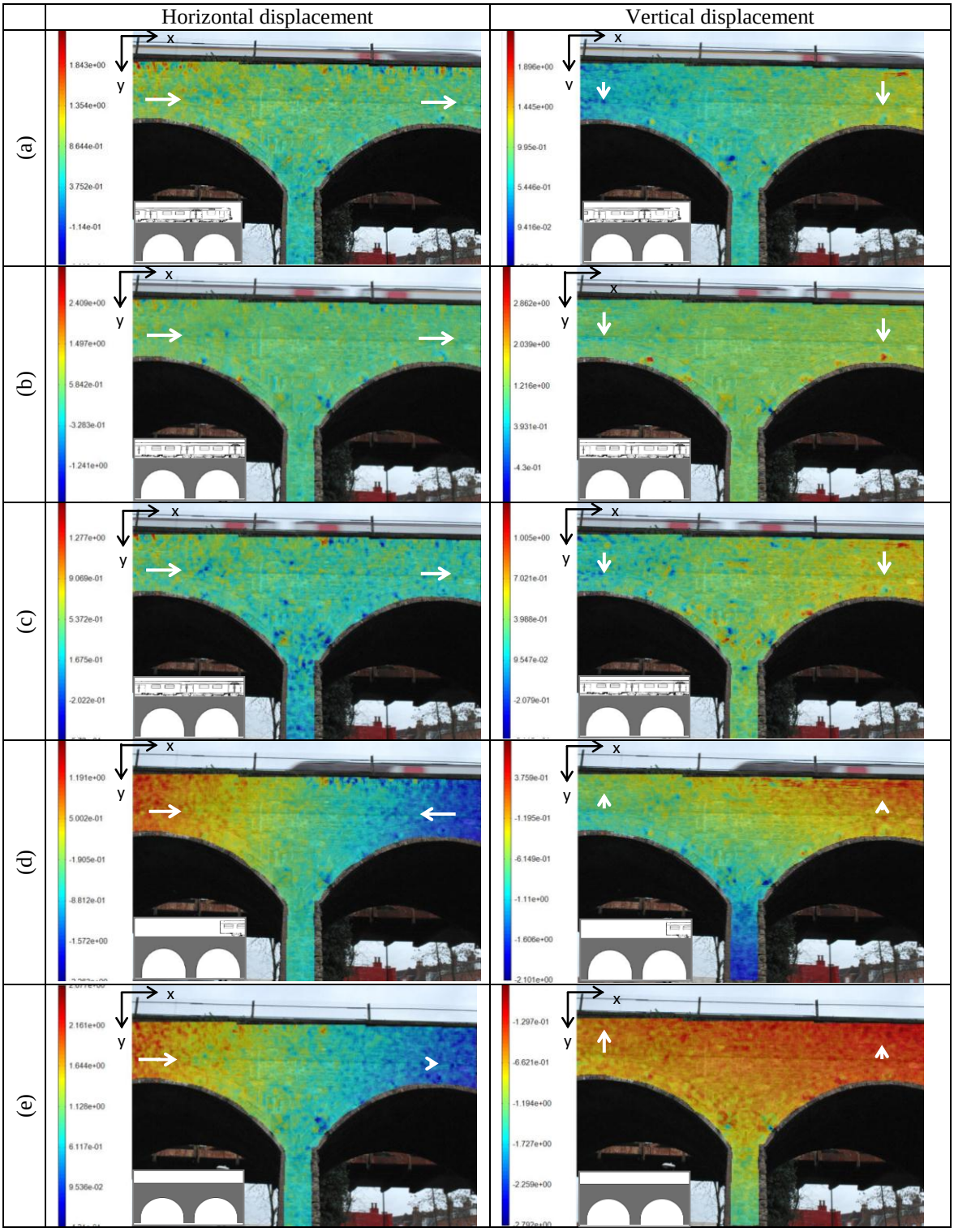

Figure 7: Horizontal and vertical displacements (vectors not to scale)

General trends for selected areas of the structure may be easier interpreted by plotting time-deflection curves. Figure 8 shows the horizontal and vertical displacements against train locations for the crown of the 1st and 2nd spans, top of the pier and the mean deflection for the entire surface area. As the train is fully over the bridge (train locations a-c) the 1st span has slightly larger horizontal movement compared to the 2nd span that is not unexpected due to the stiffening effect of the adjacent abutment. Initially, the vertical displacement of the 1st span is slightly smaller, increasing for train location b and decreasing again for location c. As the train is leaving the bridge, the 2nd span is pushed briefly backwards towards the left and again towards the right. Interestingly

enough, the 1st span keeps moving towards the right indicating the largest horizontal movement just as the train has left the bridge that is somewhat unexpected. The top of the pier and the average displacement for the entire surface area seems to follow the movement of the 2nd span relatively closely. Further details may also be extracted from the images, for example the movement of the steel strengthening plates or the rest of the pier. While it is possible to indicate numerical values for the current test, the paper only aims to demonstrate the use of DIC for laboratory and field testing, rather than carry out a detailed study of the a particular structure.

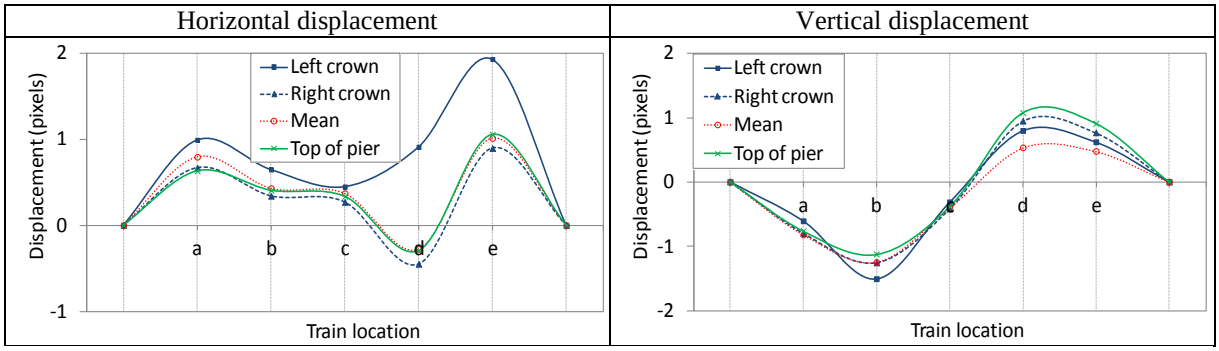

Figure 8: Horizontal (a) and Vertical (b) displacements vs. train location (see Figure 9a-e)

5. CONCLUSIONS

Unlike traditional NDT techniques measuring individual points on the structure, Digital Image Correlation is a low-cost, non-contact optical technique that allows deflection, stress and strain distribution to be recorded over the entire surface. Efficacy of the technique for masonry has been assessed through laboratory experiments on small-scale masonry specimens and for masonry arch bridges under field conditions. The technique proved suitable for measuring crack location and displacements on small-scale specimens and proved particularly useful for measuring crack propagation and indicating changes in behaviour under loading. A masonry arch railway bridge was monitored under live loading and allowed deformation to be visualised and measured across the surface. Time-deflection relationship proved particularly useful to identify the behaviour of any part of the structure under loading. Further work will be carried out to further correlate the DIC against other NDT techniques.

REFERENCES

[1] McCann, D.M. and Forde M.C. 2001. Review of NDT methods in the assessment of concrete and masonry structures. *NDT & E International.* 34(2), pp. 71–84.

[2] Urban Z. and Gutermann M. 2009. Assessment of masonry arch railway bridges using non-destructive in-situ testing methods. *Engineering Structures.* 31(10), pp. 2287-2298.

[3] CIRIA 2006. C656 Masonry arch bridges: condition appraisal and remedial treatment.

[4] De Santis S. and Tomor A. K. 2013. Laboratory and field studies on the use of acoustic emission for masonry bridges. *NDT & E International.* 55, pp. 64-74.

[5] Nowell, D., Paynter, R. and De Matos, P. 2010. Optical methods for measurement of fatigue crack closure: moire interferometry and digital image correlation, *Fatigue & fracture of engineering materials & structures*. 33(12), pp. 778-790.

[6] Tung, S., Shih, M. and Sung, W. 2008. Development of digital image correlation method to analyse crack variations of masonry wall. *Sadhana*. 33 (6), pp.767-779.

[7] McCormick, N. and Lord, J. 2012. Digital Image Correlation for Structural Measurements, *ICE - Civil Engineering*.

[8] Bing, P., Kemao, Q., Huimin, X. and and Anand, A. 2009. Two-dimensional digital image correlation for in-plane displacement and strain measurement: a review, *Measurement, Science and Technology*. 20 (6).

[9] Caduff, D. and Van Mier, J.G.M. 2010. Analysis of compressive fracture of three different concretes by means of 3D-digital image correlation and vacuum impregnation. *Cement and Concrete Composites*. 32(4), pp.281-290.

[10] Catholic University College Ghent, Belgium. 2012. *MatchID.* Avaliable from: http://www.matchid.org [Accessed 4 March 2013].